

EFFECTS OF SHOCK IMPINGEMENT LOCATION ON PANEL AEROELASTIC STABILITY IN MACH REFLECTION

Yiwen He¹ & Aiming Shi^{1*}

¹School of Aeronautics, Northwestern Polytechnical University, Xi'an, China

Abstract

The effects of shock impingement location on the aeroelastic stability and nonlinear responses of a two-dimensional shock-heated panel in Mach reflection are investigated through theoretical analysis. The influences of aggravated, nonuniform aerodynamic heating induced by shock waves are also investigated, which decrease the critical temperature but have no impact on the nondimensional stability boundary. The impact of shock impingement location on the stability boundary is explored, which forms the unique stability region of post-divergence flutter. Comparing the stability boundaries obtained through stability analysis and numerical simulation, the limitations of the stability analytical methods are illustrated. The evolution of the chaotic motion is observed through several nonlinear tools, indicating the complicated nonlinear features of aeroelastic response in Mach reflection. The nonlinear behaviors of the panel response also exhibit sensitivity to the shock impingement location, which is demonstrated through the largest Lyapunov exponent (LLE) and proper orthogonal modes (POMs). The research provides insight into the aeroelastic behavior of shock-heated panels in Mach reflection, which has important implications for the design of high-speed aircraft structures.

Keywords: aeroelasticity, thermal stress, shock reflection, Chaos

1. Introduction

Due to the lightweight requirement of high-speed vehicles, thin, flexible panels are widely equipped, which leads to the risks of undesirable aeroelastic problems threatening structural safety. Shock waves are commonly encountered when traveling at supersonic/hypersonic speed, which cause severe pressure and thermal loads on the flexible panels, seriously increasing the risk of aeroelastic damage.

In recent years, the aeroelastic performance of the panel impinged by oblique shock, which forms either regular reflection or Mach reflection, has aroused the interest of researchers. For regular shock reflection, the crucial role of shock impingement location in the aeroelastic behaviors of the panel has been revealed [1], which displays a nonmonotonic impact on the stability boundary. For Mach reflection, the effects of shock impingement location are still under question, which may significantly alter the aeroelastic stability and response considering the complicated flow field formed by the Mach stem shock. Furthermore, the panel in Mach reflection displays multiple aeroelastic responses, whose stability boundary is much more complicated [2]. Thus, it is necessary to investigate the effects of shock impingement location on the panel aeroelastic behaviors in Mach reflection. Besides, across the shock waves, the temperature increases dramatically and forms a nonuniform temperature distribution on the panel. In the previous research[3, 2], the temperature distribution is either ignored or assumed to be uniform. Therefore, a discussion on the thermal stress brought by shock-induced heating will be valuable in disclosing the impacts of nonuniformity and aggravation of the heat field.

Due to the nonlinear factors in the panel aeroelastic systems, the aeroelastic response contains rich nonlinear characteristics, among which chaotic motions are of special interest. Dowell [4, 5] revealed the chaotic motions of a fluttering buckled plate and summarized effective descriptors to observe the

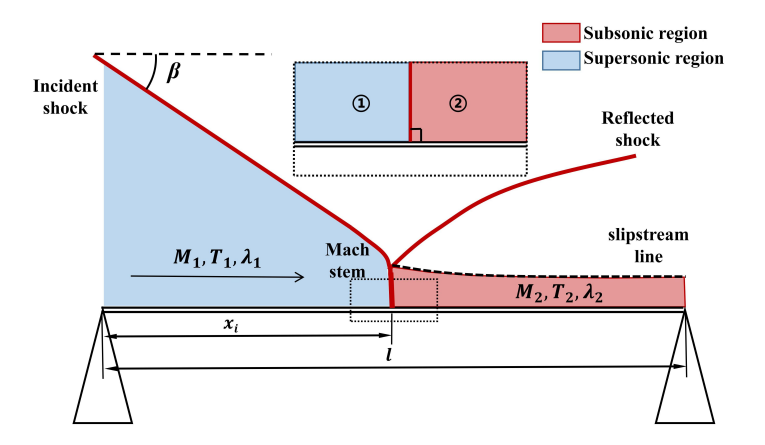


Figure 1 – Schematic of a panel impinged by an oblique shock forming Mach reflection.

evolution of chaos, including Poincare maps, phase diagrams, etc. Besides, the largest Lyapunov exponent (LLE) is subsequently introduced as a quantitative measure to determine chaotic motions. The investigation of chaos was then extended to various panels, such as viscoelastic panels [6] and damaged panels [7], and different flow conditions, such as subsonic flow [8] and turbulent flow [9]. For the shock-dominated flows, the involvement of shock waves will introduce additional nonlinearity into the aeroelastic system, enriching the nonlinear characteristics of its response. The chaotic motion of the panel in Mach reflection might be more complicated, which is worth further investigation.

This paper presents an aeroelastic model for a two-dimensional panel subjected to shock-induced heating in Mach reflection. A detailed discussion is conducted to illustrate the impact of aggravated, non-uniform temperature distribution induced by shock waves. The stability boundary is exploited, which proved sensitive to the shock impingement location. A comparison is conducted between analytical results and numerical results, which demonstrates the limitation of the stability analytical methods. A comprehensive description of the chaotic motion is provided to reveal the complex nonlinear features of aeroelastic response in Mach reflection, demonstrating its sensitivity to shock impingement location.

2. Model Formulation

A schematic of the panel impinged by an oblique shock wave forming Mach reflection is depicted in Figure 1. β represents the shock angle of the incident shock and x_i represents the shock impingement location on the panel. To investigate the panel aeroelastic stability, the emphasis is on the area near the incident point of the oblique shock. Only the flowfield near the panel is taken into consideration. The Mach stem shock can be approximately treated as a normal shock, which divides the area into a supersonic region and a subsonic region.

2.1 Aerodynamic pressure theory

For a supersonic region, the quasi-steady first-order piston theory is employed to evaluate the unsteady aerodynamic pressure.

$$q_a = \frac{2q_{\infty}}{\sqrt{M_{\infty}^2 - 1}} \left(\frac{\partial w}{\partial x} + \frac{M_{\infty}^2 - 2}{M_{\infty}^2 - 1} \frac{1}{U_{\infty}} \frac{\partial w}{\partial t} \right) \tag{1}$$

For a subsonic region behind the Mach stem shock, where the flow is compressible, the compressibility-corrected potential theory is applied. The compressibility-corrected potential theory is a modification of classical potential theory by introducing a Prandtl-Glauert compressibility correction, which has been verified and proved to be valid and efficient [2].

$$q_{a} = \frac{1}{\sqrt{1 - M_{\infty}^{2}}} \left[\frac{\rho_{\infty}}{\pi} \int_{0}^{l} \left(\frac{\partial^{2} w}{\partial t^{2}} + U^{2} \frac{\partial^{2} w}{\partial t \partial x} \right) \ln \left| \frac{x - \xi}{l} \right| d\xi + \frac{\rho_{\infty}}{\pi} \oint \left(U \frac{\partial w}{\partial t} + U^{2} \frac{\partial w}{\partial x} \right) \frac{1}{x - \xi} d\xi \right]$$
(2)

2.2 Structural theory

In this paper, the emphasis is on the panel stability boundary with thermal stress considered, thus the static pressure differential across the panel is ignored for simplicity. According to the von-Karman large deflection plate theory, the coupled partial differential governing equation of motion for the panel is established.

$$D\frac{\partial^{4} w}{\partial x^{4}} - (N_{x} - N_{x}^{T})\frac{\partial^{2} w}{\partial x^{2}} + c\frac{\partial w}{\partial t} + \rho h\frac{\partial^{2} w}{\partial t^{2}} + q_{a} = 0, \quad N_{x} = \frac{Eh}{2l(1 - v^{2})} \int_{0}^{l} \left(\frac{\partial w}{\partial x}\right)^{2} dx \tag{3}$$

Since the panel in Mach reflection may lose its stability in the form of divergence, it is necessary to include a structural damping c into the system to complete the structural model. The term N_x^T represents the thermal stress induced by temperature rise caused by aerodynamic heat, for which a detailed discussion will be presented in the following text.

The governing equation for the panel can be transformed to the dimensionless form as

$$\frac{\partial^2 W}{\partial \tau^2} - (R_x - R_x^T) \frac{\partial^2 W}{\partial \xi^2} + \frac{\partial^4 W}{\partial \xi^4} + c \frac{\partial W}{\partial \tau} + \bar{q}_a = 0$$
(4)

where the details of the dimensionless parameters are defined in Appendix A.

To solve the 4th-order partial differential equation, the Galerkin method is employed to discretize the continuous system into a multi-degree-of-freedom system.

2.3 Thermal stress

Since a thin panel is considered here, the temperature is assumed to be invariable across the panel in the thickness direction. The temperature distribution in the panel along the length direction is assumed to be consistent with the temperature distribution of the flowfield after heating. Thus, employing the quasi-steady thermal stress theory, the thermal stress caused by the temperature rise can be expressed as

$$N_x^T = \int_0^l \frac{Eh\alpha}{l} \Delta T(x) dx = \frac{Eh\alpha}{l} \left[\int_0^{x_T} \Delta T_1 dx + \int_{x_T}^l \Delta T_2 dx \right]$$
 (5)

where the $\Delta T_2(x)$ can be obtained from normal shock theory.

Usually, the temperature status of the panel are described by the nondimensional ratio $\Delta T/\Delta T_{cr}$, which can be obtained through

$$\frac{\Delta T}{\Delta T_{cr}} = \frac{R_x^T}{\pi^2} \tag{6}$$

And the stability boundary considering thermal stress are expressed in terms of λ vs $\Delta T/\Delta T_{cr}$. Xue and Mei [10, 11] conducted a detailed investigation on the temperature effects on the panel aeroelastic stability. It is found that for a two-dimensional panel with different temperature distribution $\Delta T(x)_a$ and $\Delta T(x)_b$, for the case of same temperature ratio

$$\frac{\Delta T(x)_a}{\Delta T_{cr}(x)_a} = \frac{\Delta T(x)_b}{\Delta T_{cr}(x)_b} \tag{7}$$

The panel responses are identical, except for in-plane displacements. And the stability boundary depicted in terms of λ vs $\Delta T/\Delta T_{cr}$ are the same for different temperature distribution. It demonstrates that with $\Delta T/\Delta T_{cr}$ to describe the thermal stress, the results for nonuniform temperature distribution will make no difference with the one for uniform temperature distribution. However, the dramatic increase of the temperature across the shock waves is nonnegligible, which will result in a lower critical temperature. For a simply supported two-dimensional panel the critical temperature can be obtained from the expression.

$$\int_0^l \frac{Eh\alpha}{l} \Delta T_{cr}(x) dx = \frac{\pi^2 D}{l^2}$$
 (8)

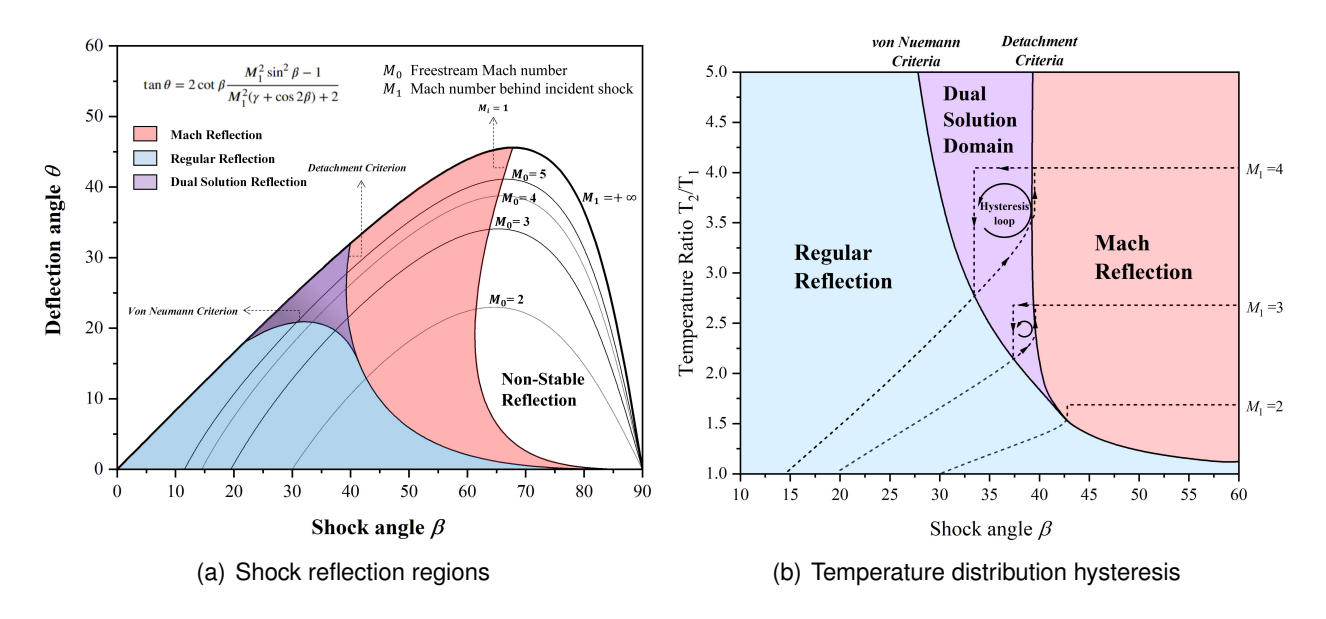


Figure 2 – Shock-induced hysteresis phenomenon in temperature distribution

The relation between the critical temperature in shock reflections and that in supersonic flow can then be established, which can be expressed as

$$\Delta T_{cr} = \frac{\Delta T_{cr,0}}{T_2/T_1(l - x_T) + x_T} \tag{9}$$

where $\Delta T_{cr.0}$ represent the critical temperature in entire supersonic flow.

Despite no impact of non-uniformity of the temperature distribution, the temperature increase caused by shock waves will result in the increase of critical temperature. Besides, in the previous research [12], it was found that the transition between Mach reflection and regular reflection will induce an aeroelastic hysteresis for the panel. Similarly, induced by the shock-reflection transition, a hysteresis will be formed for the temperature ratio T_2/T_1 and subsequently for the critical temperature. As shown in Figure 2, the temperature ratio across the shock reflection is plotted in the oblique-shock frame to exhibit the hysteresis phenomenon. The temperature ratio for the Mach reflection is larger than that for regular reflection. Due to the existence of the dual solution region, a hysteresis loop is formed, which will then induce a hysteresis in the critical temperature.

2.4 Galerkin Approach

Considering the simply supported boundary conditions, the lateral displacement can be expressed as

$$W(\xi,\tau) = \sum_{i=1}^{N} q_i(\tau) \sin(i\pi\xi)$$
(10)

where $q_i(\tau)$ are the generalized coordinates.

By substituting the expression into Equation 4 and multiplying by another set of the primary spatial function and integrating from 0 to 1, the discrete motion equations are obtained.

$$\frac{q_{j}(j\pi)^{4}}{2} - \frac{q_{j}R_{x}^{T}(j\pi)^{2}}{2} + 3q_{j}(j\pi)^{2} \left[\sum_{r=1}^{N} \frac{q_{r}^{2}}{2} (r\pi)^{2} \right] + \frac{1}{2}\ddot{q}_{j} + A + C\dot{q}_{j} = 0$$
(11)

The equation above is a set of nondimensional ordinary differential equations, where the term A represents the aerodynamic pressures terms with details given in Appendix B. By assuming that $\dot{q}_i = q_{i+N}$, the motion equations are converted into 1st-order ordinary differential equations, which are solved by the 4th-order Runge-Kutta direct numerical integration method.

3. Stability Analysis

Bolotin et al. [13] clearly illustrated a systematic approach to investigate the instability of an elastic panel, which is then widely applied to deal with the aeroelastic stability of panels in different flow conditions [14]. In the present stability analysis, the analytical approach is also applied, including the Lyapunov indirect Method and buckled equilibrium modes. Since the nonuniform temperature distribution has no influence on the aeroelastic boundary of two-dimensional panels, the stability boundaries in this paper is still plotted in terms of λ vs $\Delta T/\Delta T_{cr}$.

3.1 Lyapunov Indirect Method

To study the aeroelastic stability of the panel, the nonlinear ordinary differential equations of a two-mode (N = 2) panel aeroelastic system is established as

$$\begin{split} \dot{q}_{1} &= q_{3}, \quad \dot{q}_{2} = q_{4} \\ \dot{q}_{3} &= -\pi^{2}(\pi^{2} - R_{x}^{T})q_{1} - 3\pi^{2}q_{1}\left(\pi^{2}q_{1}^{2} + 4\pi^{2}q_{2}^{2}\right) - Cq_{3} \\ &- 2\lambda_{1}q_{2}\left[\cos(\pi\xi_{T}) - \frac{1}{3}\cos(3\pi\xi_{T}) - \frac{2}{3}\right] - \lambda_{1}q_{1}\sin^{2}(\pi\xi_{T}) \\ &- \frac{\sqrt{\lambda_{1}R_{m,1}}}{\pi}q_{4}\left[\sin(\pi\xi_{T}) - \frac{1}{3}\sin(3\pi\xi_{T})\right] - \sqrt{\lambda_{1}R_{m,1}}q_{3}\left[\xi_{T} - \frac{\sin(2\pi\xi_{T})}{2\pi}\right] \\ &+ \frac{2\lambda_{2}}{\sqrt{1-M_{2}^{2}}}q_{2}\left[\frac{1}{3}\sin(3\pi\xi_{T}) - \sin(\pi\xi_{T})\right] + \frac{\lambda_{2}}{\sqrt{1-M_{2}^{2}}}q_{1}\left[\pi(1-\xi_{T}) + \frac{1}{2}\sin(2\pi\xi_{T})\right] \\ &- \frac{2\sqrt{\mu_{2}\lambda_{2}}}{\pi\sqrt{1-M_{2}^{2}}}q_{4}\left[\frac{1}{3}\cos(3\pi\xi_{T}) - \cos(\pi\xi_{T}) - \frac{2}{3}\right] - \frac{\sqrt{\mu_{2}\lambda_{2}}}{\pi\sqrt{1-M_{2}^{2}}}q_{3}\left[\cos(2\pi\xi_{T}) - 1\right] \\ \dot{q}_{4} &= -4\pi^{4}(4\pi^{2} - R_{x}^{T})q_{2} - 12\pi^{2}q_{2}\left(\pi^{2}q_{1}^{2} + 4\pi^{2}q_{2}^{2}\right) - Cq_{4} \\ &- \lambda_{1}q_{1}\left[-\cos(\pi\xi_{T}) - \frac{1}{3}\cos(3\pi\xi_{T}) + \frac{4}{3}\right] - \lambda_{1}q_{2}\sin^{2}(2\pi\xi_{T}) \\ &- \frac{\sqrt{\lambda_{1}R_{m,1}}}{\pi}q_{3}\left[\sin(\pi\xi_{T}) - \frac{1}{3}\sin(3\pi\xi_{T})\right] - \sqrt{\lambda_{1}R_{m,1}}q_{4}\left[\xi_{T} - \frac{\sin(4\pi\xi_{T})}{4\pi}\right] \\ &+ \frac{\lambda_{2}}{\sqrt{1-M_{2}^{2}}}q_{1}\left[\frac{1}{3}\sin(3\pi\xi_{T}) - \sin(\pi\xi_{T})\right] + \frac{\lambda_{2}}{\sqrt{1-M_{2}^{2}}}q_{2}\left[2\pi(1-\xi_{T}) + \frac{1}{2}\sin(4\pi\xi_{T})\right] \\ &- \frac{2\sqrt{\mu_{2}\lambda_{2}}}{\pi\sqrt{1-M_{2}^{2}}}q_{3}\left[\frac{1}{3}\cos(3\pi\xi_{T}) + \cos(\pi\xi_{T}) + \frac{4}{3}\right] - \frac{\sqrt{\mu_{2}\lambda_{2}}}{\pi\sqrt{1-M_{2}^{2}}}q_{4}\left[\frac{\cos(4\pi\xi_{T}) - 1}{2}\right] \end{split}$$

The Jacobi matrix of the aeroelastic system at the equilibrium point of the initially flat panel $q_1 = q_2 = 0$ can be expressed as

$$J_A = \begin{pmatrix} 0 & 0 & 1 & 0 \\ 0 & 0 & 0 & 1 \\ a_{31} & a_{32} & a_{33} & a_{34} \\ a_{41} & a_{42} & a_{43} & a_{44} \end{pmatrix}$$
 (13)

where,

$$a_{31} = -\pi^{2}(\pi^{2} - R_{x}^{T}) - \lambda_{1} \sin^{2}(\xi_{T}\pi) + \frac{\lambda_{2}}{\sqrt{1 - M_{2}^{2}}} \left[\pi \left(1 - \xi_{T} \right) + \frac{1}{2} \sin(2\xi_{T}\pi) \right]$$

$$a_{32} = -2\lambda \left[\cos(\xi_{T}\pi) - \frac{1}{3} \cos(3\xi_{T}\pi) - \frac{2}{3} \right] + \frac{2\lambda_{2}}{\sqrt{1 - M_{2}^{2}}} \left[\frac{1}{3} \sin(3\xi_{T}\pi) - \sin(\xi_{T}\pi) \right]$$

$$a_{33} = -C - \sqrt{\lambda_{1}} R_{M1} \left[\xi_{T} - \frac{\sin(2\xi_{T}\pi)}{2\pi} \right] - \frac{\sqrt{\mu_{2}\lambda_{2}}}{\pi\sqrt{1 - M_{2}^{2}}} \left[\cos(2\xi_{T}\pi) - 1 \right]$$

$$a_{34} = -\frac{\sqrt{\lambda_{1}} R_{M1}}{\pi} \left[\sin(\xi_{T}\pi) - \frac{1}{3} \sin(3\xi_{T}\pi) \right] - \frac{2\sqrt{\mu_{2}\lambda_{2}}}{\pi\sqrt{1 - M_{2}^{2}}} \left[\frac{1}{3} \cos(3\xi_{T}\pi) - \frac{2}{3} - \cos(\xi_{T}\pi) \right]$$

$$\begin{split} a_{41} &= -\lambda_1 \left[\frac{4}{3} - \cos(\xi_T \pi) - \frac{1}{3} \cos(3\xi_T \pi) \right] + \frac{\lambda_2}{\sqrt{1 - M_2^2}} \left[\frac{1}{3} \sin(3\xi_T \pi) - \sin(\xi_T \pi) \right] \\ a_{41} &= -\lambda_1 \left[\frac{4}{3} - \cos(\xi_T \pi) - \frac{1}{3} \cos(3\xi_T \pi) \right] + \frac{\lambda_2}{\sqrt{1 - M_2^2}} \left[\frac{1}{3} \sin(3\xi_T \pi) - \sin(\xi_T \pi) \right] \\ a_{42} &= -4\pi^2 (4\pi^2 - R_x^T) - \lambda_1 \sin^2(2\xi_T \pi) + \frac{\lambda_2}{\sqrt{1 - M_2^2}} \left[\frac{4\pi (1 - \xi_T) + \sin(4\xi_T \pi)}{2} \right] \\ a_{43} &= -\frac{\sqrt{\lambda_1 R_{M1}}}{\pi} \left[\sin(\xi_T \pi) - \frac{1}{3} \sin(3\xi_T \pi) \right] - \frac{2\sqrt{\mu_2 \lambda_2}}{\pi \sqrt{1 - M_2^2}} \left[\frac{4}{3} + \frac{1}{3} \cos(3\xi_T \pi) + \cos(\xi_T \pi) \right] \\ a_{44} &= -C - \sqrt{\lambda_1 R_{M1}} \left[\xi_T - \frac{\sin(4\xi_T \pi)}{4\pi} \right] - \frac{\sqrt{\mu_2 \lambda_2}}{\sqrt{1 - M_2^2}} \left[\frac{\cos(4\xi_T \pi) - 1}{2\pi} \right] \end{split}$$

The characteristic polynomial of the Jacobi matrix can be expressed as

$$\lambda^4 + A_1 \lambda^3 + A_2 \lambda^2 + A_3 \lambda + A_4 = 0 \tag{14}$$

where the coefficient of each term can be expressed as: $A_1 = -a_{33} - a_{44}$, $A_2 = a_{33}a_{44} - a_{42} - a_{31}$, $A_3 = a_{42} + a_{31}a_{44} - a_{32}a_{34} - a_{41}a_{34}$, $A_4 = a_{31}a_{42} - a_{32}a_{41}$.

Only when all the roots of Equation 14 have negative real parts, the aeroelastic response of the panel will be stable. Thus, the Routh-Hurwitz criterion is employed here to determine the stability of the panel aeroelastic system, which can be expressed as

$$A_1 > 0, \quad A_3 > 0, \quad A_4 > 0$$
 (15)

$$A_3(A_1A_2 - A_3) - A_1^2A_4 > 0 (16)$$

The last condition of Equation 15 and Equation 16 represents the divergence (buckling) boundary and flutter boundary, respectively. In the case of supersonic flows, the analytical expression of the stability boundaries can be obtained from the above equations. However, for the Mach reflection, the terms in the Jacobi matrix are relatively complex, which makes it difficult to obtain the analytical expression. Thus, numerical approaches are employed to solve the above equations.

3.2 Buckled Equilibrium Modes

By ignoring the time-dependent terms in Equation 12, the motion equations can be reduced to the static equilibrium equations.

$$q_{1}\left\{\pi^{2}(\pi^{2}-R_{x}^{T})+3\pi^{4}\left(q_{1}^{2}+4q_{2}^{2}\right)+\lambda_{1}\sin^{2}\left(\pi\xi_{T}\right)-\frac{\lambda_{2}}{\sqrt{1-M_{2}^{2}}}\left[\pi(1-\xi_{T})+\frac{1}{2}\sin(2\pi\xi_{T})\right]\right\}$$

$$+q_{2}\left\{2\lambda_{1}\left[\cos(\pi\xi_{T})-\frac{1}{3}\cos(3\pi\xi_{T})-\frac{2}{3}\right]-\frac{2\lambda_{2}}{\sqrt{1-M_{2}^{2}}}\left[\frac{1}{3}\sin(3\pi\xi_{T})-\sin(\pi\xi_{T})\right]\right\}=0$$

$$q_{2}\left\{4\pi^{2}(4\pi^{2}-R_{x}^{T})+12\pi^{4}\left(q_{1}^{2}+4q_{2}^{2}\right)+\lambda_{1}\sin^{2}\left(2\pi\xi_{T}\right)-\frac{\lambda_{2}}{\sqrt{1-M_{2}^{2}}}\left[2\pi(1-\xi_{T})+\frac{1}{2}\sin(4\pi\xi_{T})\right]\right\}$$

$$+q_{1}\left\{\lambda_{1}\left[-\cos(\pi\xi_{T})-\frac{1}{3}\cos(3\pi\xi_{T})+\frac{4}{3}\right]-\frac{\lambda_{2}}{\sqrt{1-M_{2}^{2}}}\left[\frac{1}{3}\sin(3\pi\xi_{T})-\sin(\pi\xi_{T})\right]\right\}=0$$

$$(17)$$

By assuming $H = 3(q_1^2 + 3q_2^2)$, the condition for the non-zero solutions existing for the static equilibrium equations can be expressed as

$$H = -\frac{5}{2} + \frac{\Delta T}{\Delta T_{cr}} \pm \sqrt{\left(3 + \frac{a_{42}^*}{4\pi^4} + \frac{a_{31}^*}{\pi^4}\right)^2 - \frac{12a_{31}^*}{\pi^4} + \frac{a_{31}^*a_{42}^*}{\pi^8} - \frac{a_{41}a_{32}}{\pi^8}}$$
(18)

where,

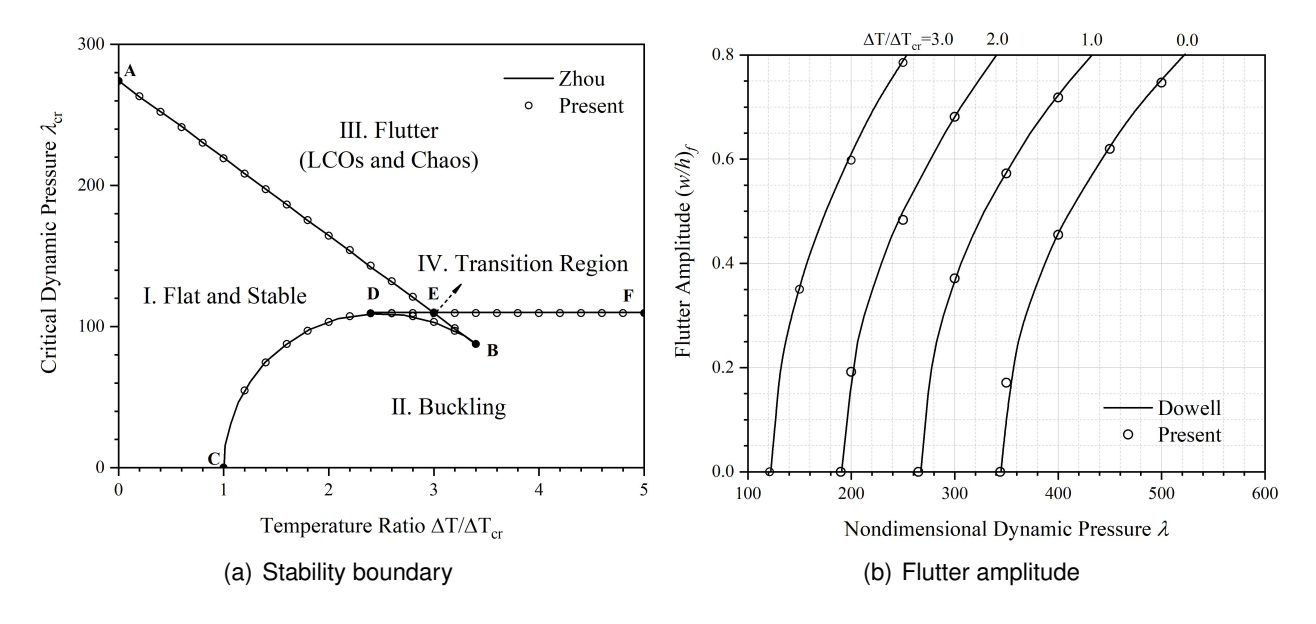


Figure 3 - Verification

$$a_{31}^{*} = \lambda_{1} \sin^{2}(\xi_{T}\pi) - \frac{\lambda_{2}}{\sqrt{1 - M_{2}^{2}}} \left[\pi \left(1 - \xi_{T} \right) + \frac{1}{2} \sin(2\xi_{T}\pi) \right] \\ a_{42}^{*} = \lambda_{1} \sin^{2}(2\xi_{T}\pi) - \frac{\lambda_{2}}{\sqrt{1 - M_{2}^{2}}} \left[\frac{4\pi \left(1 - \xi_{T} \right) + \sin(4\xi_{T}\pi)}{2} \right] \\ a_{31}^{*} = \lambda_{1} \sin^{2}(\xi_{T}\pi) - \frac{\lambda_{2}}{\sqrt{1 - M_{2}^{2}}} \left[\frac{4\pi \left(1 - \xi_{T} \right) + \sin(4\xi_{T}\pi)}{2} \right] \\ a_{31}^{*} = \lambda_{1} \sin^{2}(\xi_{T}\pi) - \frac{\lambda_{2}}{\sqrt{1 - M_{2}^{2}}} \left[\frac{4\pi \left(1 - \xi_{T} \right) + \sin(4\xi_{T}\pi)}{2} \right] \\ a_{31}^{*} = \lambda_{1} \sin^{2}(\xi_{T}\pi) - \frac{\lambda_{2}}{\sqrt{1 - M_{2}^{2}}} \left[\frac{4\pi \left(1 - \xi_{T} \right) + \sin(4\xi_{T}\pi)}{2} \right] \\ a_{31}^{*} = \lambda_{1} \sin^{2}(\xi_{T}\pi) - \frac{\lambda_{2}}{\sqrt{1 - M_{2}^{2}}} \left[\frac{4\pi \left(1 - \xi_{T} \right) + \sin(4\xi_{T}\pi)}{2} \right] \\ a_{31}^{*} = \lambda_{1} \sin^{2}(\xi_{T}\pi) - \frac{\lambda_{2}}{\sqrt{1 - M_{2}^{2}}} \left[\frac{4\pi \left(1 - \xi_{T} \right) + \sin(4\xi_{T}\pi)}{2} \right] \\ a_{31}^{*} = \lambda_{1} \sin^{2}(\xi_{T}\pi) - \frac{\lambda_{2}}{\sqrt{1 - M_{2}^{2}}} \left[\frac{4\pi \left(1 - \xi_{T} \right) + \sin(4\xi_{T}\pi)}{2} \right] \\ a_{31}^{*} = \lambda_{1} \sin^{2}(\xi_{T}\pi) - \frac{\lambda_{2}}{\sqrt{1 - M_{2}^{2}}} \left[\frac{4\pi \left(1 - \xi_{T} \right) + \sin(4\xi_{T}\pi)}{2} \right] \\ a_{31}^{*} = \lambda_{1} \sin^{2}(\xi_{T}\pi) - \frac{\lambda_{2}}{\sqrt{1 - M_{2}^{2}}} \left[\frac{4\pi \left(1 - \xi_{T} \right) + \sin(4\xi_{T}\pi)}{2} \right] \\ a_{31}^{*} = \lambda_{1} \sin^{2}(\xi_{T}\pi) - \frac{\lambda_{2}}{\sqrt{1 - M_{2}^{2}}} \left[\frac{4\pi \left(1 - \xi_{T} \right) + \sin(4\xi_{T}\pi)}{2} \right] \\ a_{31}^{*} = \lambda_{1} \sin^{2}(\xi_{T}\pi) - \frac{\lambda_{2}}{\sqrt{1 - M_{2}^{2}}} \left[\frac{4\pi \left(1 - \xi_{T} \right) + \sin(4\xi_{T}\pi)}{2} \right] \\ a_{31}^{*} = \lambda_{1} \sin^{2}(\xi_{T}\pi) - \frac{\lambda_{2}}{\sqrt{1 - M_{2}^{2}}} \left[\frac{4\pi \left(1 - \xi_{T} \right) + \sin(4\xi_{T}\pi)}{2} \right] \\ a_{31}^{*} = \lambda_{1} \sin^{2}(\xi_{T}\pi) - \frac{\lambda_{2}}{\sqrt{1 - M_{2}^{2}}} \left[\frac{4\pi \left(1 - \xi_{T} \right) + \sin(4\xi_{T}\pi)}{2} \right] \\ a_{31}^{*} = \lambda_{1} \sin^{2}(\xi_{T}\pi) - \frac{\lambda_{2}}{\sqrt{1 - M_{2}^{2}}} \left[\frac{4\pi \left(1 - \xi_{T} \right) + \sin(4\xi_{T}\pi)}{2} \right] \\ a_{31}^{*} = \lambda_{1} \sin^{2}(\xi_{T}\pi) - \frac{\lambda_{2}}{\sqrt{1 - M_{2}^{2}}} \left[\frac{4\pi \left(1 - \xi_{T} \right) + \sin(4\xi_{T}\pi)}{2} \right] \\ a_{31}^{*} = \lambda_{1} \sin^{2}(\xi_{T}\pi) - \frac{\lambda_{2}}{\sqrt{1 - M_{2}^{2}}} \left[\frac{4\pi \left(1 - \xi_{T} \right) + \sin(4\xi_{T}\pi)}{2} \right] \\ a_{31}^{*} = \lambda_{1} \sin^{2}(\xi_{T}\pi) - \frac{\lambda_{2}}{\sqrt{1 - M_{2}^{2}}} \left[\frac{4\pi \left(1 - \xi_{T} \right) + \sin(4\xi_{T}\pi)}{2} \right] \\ a_{31}^{*} = \lambda_{1} \sin^{2}(\xi_{T}\pi) - \frac{\lambda_{2}}{\sqrt{1 - M_{2}^{2}}} \left[\frac{4\pi \left(1 - \xi_{T} \right) + \sin(4\xi_{T}\pi)$$

To ensure H as a real root, the following condition must be satisfied

$$\left(3 + \frac{a_{42}^*}{4\pi^4} + \frac{a_{31}^*}{\pi^4}\right)^2 - \frac{12a_{31}^*}{\pi^4} + \frac{a_{31}^*a_{42}^*}{\pi^8} - \frac{a_{41}a_{32}}{\pi^8} \ge 0 \tag{19}$$

Once is Equation 19 no more satisfied, there exists no non-zero solution for the static equilibrium equations, which means it is impossible for the panel to be stabilized in the form of a buckled panel. Thus, the equation represents a part of the buckling boundary.

A further discussion on the solution situation of the static equilibrium equations will reveal another part of the buckling boundary, which is the same as the one obtained from Equation 15. Besides, the solutions determine the situation of the equilibrium points and their stability in the stability plane. Since we focus on the stability boundaries, the situation of the equilibrium points and their stability is not discussed in the paper.

3.3 Verification

To verify the methodologies and illustrate the stability regions, the stability boundary of the elastic panel in the entire supersonic flow is plotted and compared with the previous result obtained by Zhou et al [14]. The panel exposed to the entire supersonic flow is achieved by moving the shock impingement location to the trailing edge $\xi_T = 1.0$ in the preset aeroelastic model.

As shown in Figure 3(a), the plane is divided by the stability boundaries into four regions with different stability situations. (I) Flat and Stable (AEDC): The panel will not lose its stability and remain stable in the form of a flat panel. (II) Buckling (CDBEF): The panel will lose its static stability in the form of buckling. (III) Flutter (AEF): The panel will lose its dynamic stability in the form of flutter, including limit cycle oscillations (LCOs) and chaotic motion. (IV) Transition Region (DEB): The panel will be stable in the form of a flat or be statically unstable in the form of a post-buckled panel due to multiple asymptotically stable equilibrium points.

As shown in Figure 3(b), the flutter amplitude of the panel with different temperature ratios $\Delta T/\Delta T_{cr}$ in the supersonic flow are plotted and compared with the results obtained by Dowell[15]. The panel aeroelastic responses are calculated with a four-mode aeroelastic system with the 4th-order Runge-Kutta method. It can be seen that both the stability region and flutter amplitude calculated from the present model correspond well with the previous results in the literature.

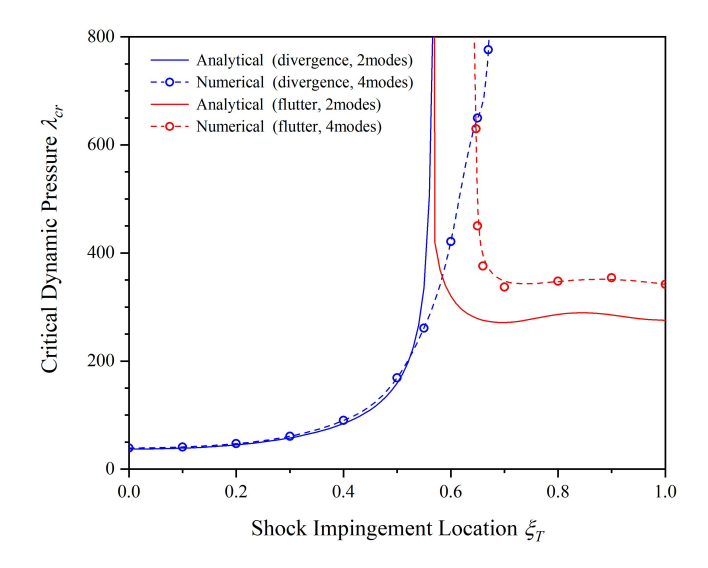


Figure 4 – Stability boundary varying with shock impingement location

4. Results and Discussion

4.1 Stability Boundary

Before the introduction of thermal stress, the stability boundary varying with shock impingement location is plotted in Figure 4. The divergence (buckle) and flutter boundary are indicated with blue and red curves, respectively. The analytical results are obtained through stability analysis and the numerical results are calculated through the 4th-order Runge-Kutta numerical method with four-mode aeroelastic system.

The shock impingement location, determining the instability situation of the panel, is a crucial factor for the panel aeroelastic stability in Mach reflection. With the Mach stem shock impinging at the front portion, the panel displays divergence instability. While, with the Mach stem shock impinging at the rear portion, the panel exhibits flutter instability. Despite different orders of aeroelastic systems, the analytical and numerical results correspond well with shock impingement location at $0 < \xi_T < 0.5$. However, as the shock impingement location further increases, differences emerge: The critical dynamic pressure for divergence increases dramatically when the shock impingement location approaches $\xi_T = 0.55$ for the analytical results, but for the numerical results, it does not increase remarkably until $\xi_T = 0.67$. For the flutter boundary, the numerical results are larger than the analytical results, but the trend corresponds well, which is consistent with the situation for the panel in regular reflection [16].

More importantly, the divergence boundary and flutter boundary intersect near $\xi_T=0.65$ for the numerical results. Above the intersection point of the two boundaries, the panel exhibits both divergence instability and flutter boundary, which is the so-called post-divergence flutter instability. Below the intersection point, despite a large freestream dynamic pressure, the panel remains stable, which suggests a strategy to implement aeroelastic control. By reasonably arranging the shock impingement location, the divergence or flutter instability can be suppressed and even eliminated. However, for the analytical results, the two boundaries intersect near $\xi_T=0.55$ and increase dramatically after the intersection, resulting in barely any post-divergence flutter region.

Through the Lyapunov indirect method, the aeroelastic stability boundary can be calculated rapidly, which can reflect the trend of critical dynamic pressure varying with shock impingement location approximately. However, the Lyapunov method can only deal with the two-mode aeroelastic model, resulting in a lack of accuracy. Especially for the panel in Mach reflection, the stability boundary obtained through the Lyapunov indirect method cannot reflect the location of the intersection between divergence/flutter boundaries and the subsequent post-divergence flutter instability properly.

Considering the crucial impact of shock impingement location on the stability situation of the panel, the stability boundaries of the shock-heated panel with different shock impingement locations are plotted in Figure 5. With shock impinging at the leading portion of the panel, there exists only the buckling boundary, which decreases with increasing temperature. With shock impinging at the trailing

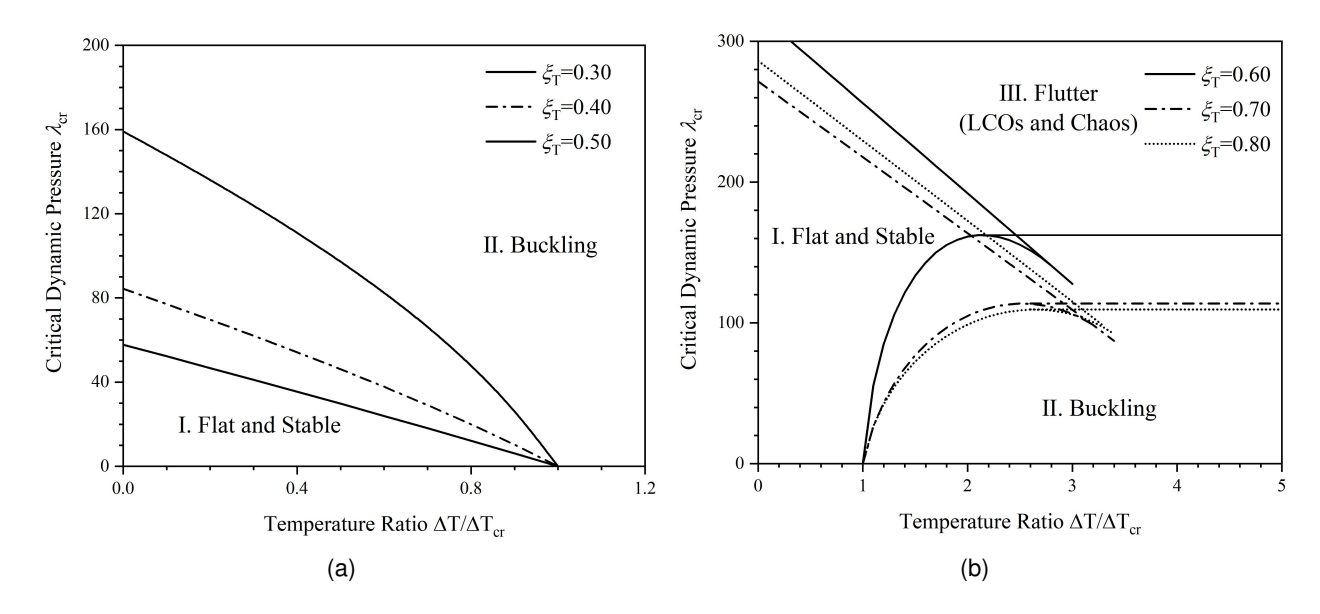


Figure 5 – Stability Boundary varying with temperature ratio with different shock impingement locations

portion of the panel, the stability boundary distribution is similar to that for supersonic flow. The critical dynamic pressure for buckle boundary decreases with increasing shock impingement location. However, the flutter boundary varies nonmonotonously with increasing shock impingement location, which corresponds with the tendency exhibited in Figure 4.

4.2 Chaotic/Periodic Motions

To investigate the impact of shock impingment location on the nonlinear behaviors of the panel, the aeroelastic responses are plotted, accompanied by different nonlinear descriptors, as shown in Figure 6. The phase diagram is plotted, where the red dots indicate the Poincáre points obtained with identifying/event point $\xi = 0.25$. The fast Fourier transform (FFT) is employed to calculate the frequency spectra. Here, the temperature increase $\Delta T/\Delta T_{cr}=5$ and dynamic pressure $\lambda=150$ are used. It is noted that the shock impingement location $\xi_T = 1.0$ correspond to the situation in the supersonic flow without shock impingement. For $\xi_T = 1.0$, the characteristics of chaotic motions are observed in the time history and phase diagram, the Poincáre points displays a cloud of discrete points, further demonstrating a chaotic motion, and visualizes the existence of strange attractors. The frequency spectra have a broad frequency bandwidth, which shows the features of a random signal. With the shock impingement location moving to $\xi_T = 0.9$, the chaotic motion is transformed to a 3periodic limit cycle oscillation, which is indicated by the three discrete Poincáre points. The frequency content is also regulated in the frequency spectra. Despite the significant regulation in the nonlinear behavior, the flutter amplitude hardly changes. However, as the shock impingement location further decreases, the chaotic motions emerge again for $\xi_T = 0.8$ and $\xi_T = 0.7$. The phase diagram and frequency spectra display different characteristics for the two shock impingement location, indicating the effects of shock impingement location on the nonlinear characteristics of the panel.

To further disclose the sensitivity of nonlinear aeroelastic response to the shock impingement location, the largest Lyapunov exponent (LLE) is applied, which provides a quantitative indicator for the chaotic motions. The tendency of LLE varying with shock impingement location is plotted in Figure 7. It can be seen that LLE varies sharply with shock impingement location, indicating the alteration of the nonlinear characteristics of the panel response. An appropriate shock impingement location can regular the nonlinear behaviors, reducing the chaotic motions to regular motions. Despite a similar flutter amplitude, the variation in the shock impingement location results in a alteration in the nonlinear behaviors of the panel in Mach shock reflection.

In recent years, data-driven modal decomposition methods have served as a technique in fluidstructure interaction problems for extracting physically important features. Especially for the panel

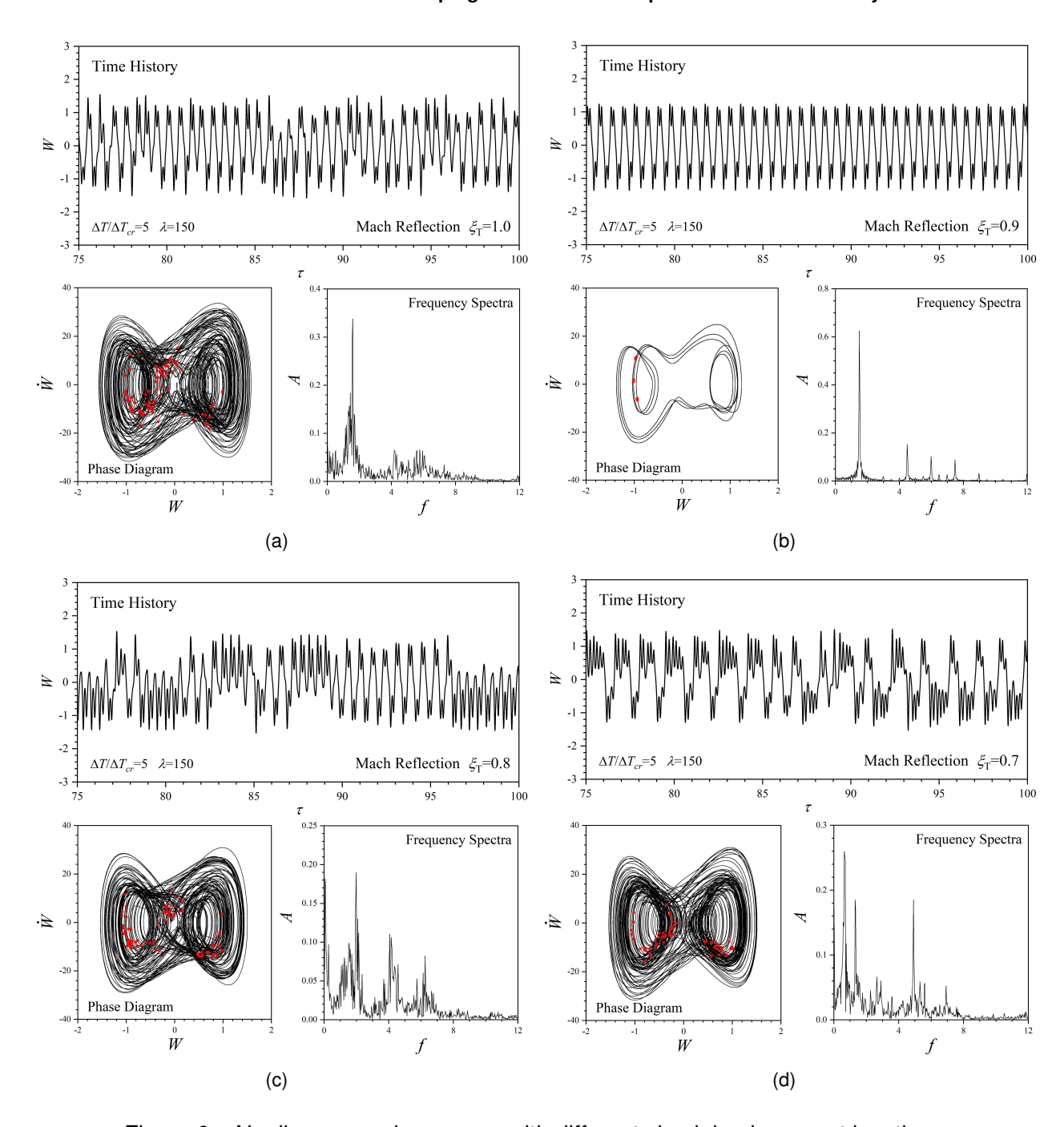


Figure 6 – Nonlinear panel response with different shock impingement locations

aeroelastic problems in shock-dominated flow, the application of modal decomposition analysis provided valuable insights into the underlying physics [17, 18]. To further explore the influence of viscoelastic damping on the nonlinear behaviors of the panel, proper orthogonal decomposition modes (POMs), as one of the most representative modal decomposition approaches, are applied here. The panel aeroelastic responses calculated with $\lambda=150$ and $\Delta T/\Delta T_{cr}=5$ are chosen as the temporal snapshots. For concision, the detailed procedure for POMs is omitted here, for which Taira et al. [19] provided a detailed description of its algorithm. The energy distribution and modal shapes of POMs with different shock impingement locations are plotted in Fig.8. The POMs are ranked in the order of importance depending on their energy distribution. From Fig.8(a), it can be seen that the POMs provide a concise description of the panel response with high efficiency, for which the first two modes occupy most of the energy contribution. Thus, only the first two dominant POMs are analyzed here. It can be seen that the variation in shock impingement location results in a significant alteration of the modal shapes.

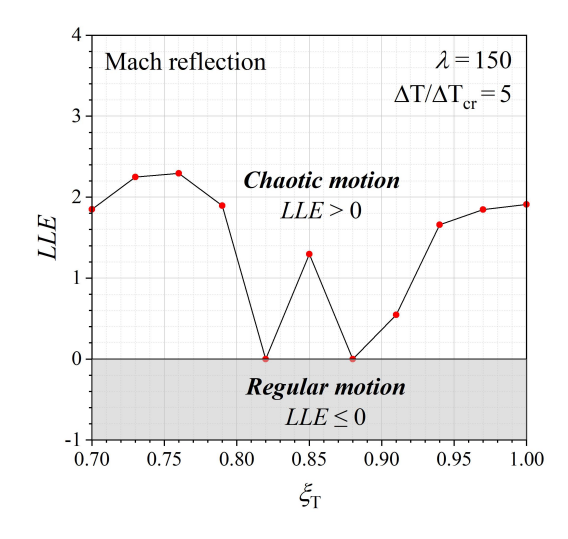


Figure 7 – Largest Lyapunov exponent varying with shock impingement location

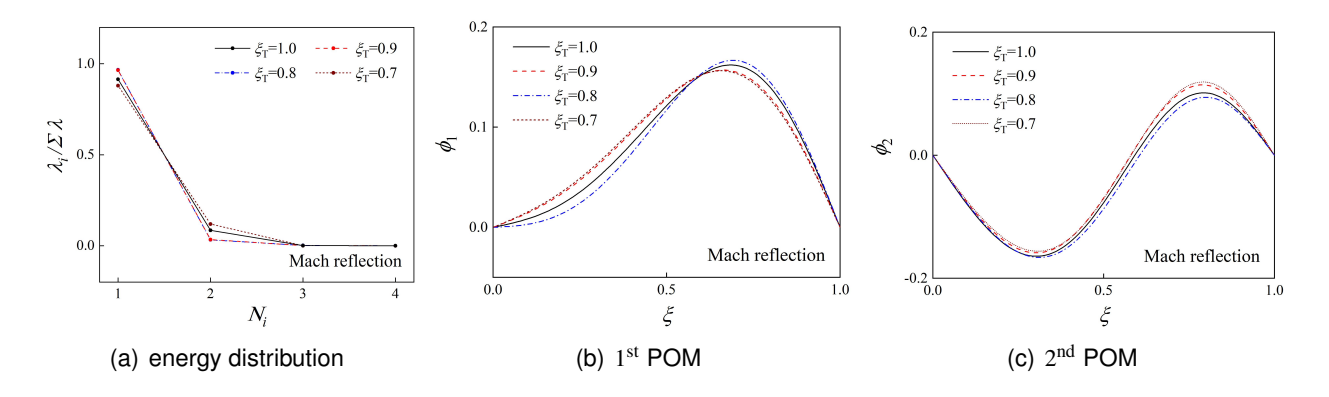


Figure 8 – Modal energy and shapes of POMs with different shock impingement location

5. Conclusions

In this paper, the aeroelastic stability and nonlinear response of a two-dimensional shock-heated panel with Mach stem shock impingement are investigated. The effect of shock impingement location on the aeroelastic behaviors is investigated in detail. The main conclusions are as follows.

- 1) Although the shock-induced nonuniform temperature distribution has no impact on the nondimensional aeroelastic stability boundary for the two-dimensional panel, the critical buckling temperature is lowered due to the temperature rise across the shock waves. However, the nonuniformity of temperature distribution may influence the stability boundary of the three-dimensional panel, which is worth further investigation. Furthermore, the potential hysteresis phenomenon in the temperature distribution may further aggravate the panel aeroelastic hysteresis, resulting in an enlarged gap between the aeroelastic performance in Mach shock reflection and regular shock reflection.
- 2) The shock impingement location plays a crucial role in the panel aeroelasticity in Mach reflection, determining the instability form. As the shock impinges at its front 2/3 portion, the panel displays divergence instability; As the shock impinges at its rear 1/3 portion, the panel displays flutter instability; As the shock impinges near its 2/3 chord, the panel displays post-divergence flutter instability. By arranging the shock impingement location, a control strategy might be developed to suppress aeroelastic instability.
- 3) The shock impingement location significantly alters the nonlinear characteristics of the panel aeroelastic response, whose tendency is nonmonotonic and relatively complicated. Despite similar flutter amplitude, the chaotic motion can be reduced to regular motions with an appropriate shock impingement location. The largest Lyapunov exponent and proper orthogonal modes prove efficient in revealing the sensitivity of nonlinear behaviors to the systemic parameters.

6. Contact Author Email Address

This paper is submitted to participate in the John McCarthy Student Award. The first author, Yiwen He, is a PhD student of Northwestern Polytechnical University.

Email: sam@nwpu.edu.cn (Prof. Aiming Shi)

7. Copyright Statement

The authors confirm that they, and/or their company or organization, hold copyright on all of the original material included in this paper. The authors also confirm that they have obtained permission, from the copyright holder of any third party material included in this paper, to publish it as part of their paper. The authors confirm that they give permission, or have obtained permission from the copyright holder of this paper, for the publication and distribution of this paper as part of the ICAS proceedings or as individual off-prints from the proceedings.

Appendix A. Nondimensional Parameters

$$\xi = \frac{x}{l}$$

$$\mu = \frac{\rho l}{\rho_m h}$$

$$\tau = t \sqrt{\frac{D}{\rho h l^4}}$$

$$R_x = \frac{N_x l^2}{D} = 6 \int_0^1 (\frac{\partial W}{\partial \xi})^2 d\xi$$

$$W = \frac{w}{h}$$

$$q_a = \frac{l^4}{Dh} q_a$$

$$\lambda_1 = \frac{2q_1 l^3}{\sqrt{M_1^2 - 1D}}$$

$$\lambda_2 = \frac{2q_2 l^3}{D}$$

$$R_m = \frac{\mu (M^2 - 2)^2}{(M^2 - 1)^{\frac{5}{2}}}$$

Appendix B. Aerodynamic Terms

The aerodynamic pressure term A can be expressed as follows.

$$A = A_1 + A_2 + A_3 + A_4 + A_5 + A_6 + A_7 + A_8$$

where A_1 to A_4 correspond to the aerodynamic terms ahead of the incident shock and A_5 to A_8 correspond to the aerodynamic terms behind the Mach stem shock.

In the supersonic region

In the subsonic region

$$\begin{split} A_1 &= \lambda_1 \sum_{i=1}^N q_i(i\pi) \left\{ \frac{\cos[(i-j)k\pi]}{2(i-j)\pi} - \frac{\cos[(i+j)k\pi]}{2(i+j)\pi} - \frac{j}{(i^2-j^2)\pi} \right\} \\ A_5 &= \frac{1}{\sqrt{1-M_2^2}} \sum_{i=1}^N \left[-\frac{\mu h}{i\pi} \ddot{q}_i + \lambda_2(i\pi) q_i \right] \left\{ \frac{\sin[(i+j)\pi k]}{2(i+j)\pi} - \frac{\sin[(i-j)\pi k]}{2(i-j)\pi} \right\} \\ A_2 &= \frac{1}{2} \lambda_1 q_j \sin^2(jk\pi) \\ A_3 &= \sqrt{\lambda_1 R_{M1}} \sum_{i=1}^N \dot{q}_i \left[\frac{\sin[(i-j)k\pi]}{2(i-j)\pi} - \frac{\sin[(i+j)k\pi]}{2(i+j)\pi} \right] \\ A_7 &= -\frac{2\sqrt{\mu_2 \lambda_2}}{\sqrt{1-M_2^2}} \sum_{i=1}^N \dot{q}_i \left\{ \frac{j(-1)^{i+j}}{(i^2-j^2)\pi} + \frac{\cos[(i+j)k\pi]}{2(i+j)\pi} - \frac{\cos[(i-j)k\pi]}{2(i-j)\pi} \right\} \\ A_4 &= \frac{1}{2} \sqrt{\lambda_1 R_{M1}} \dot{q}_j \left[k - \frac{\sin(2jk\pi)}{2j\pi} \right] \\ A_8 &= -\frac{2\sqrt{\mu_2 \lambda_2}}{\sqrt{1-M_2^2}} \dot{q}_j \left[\frac{\cos(2jk\pi) - 1}{4j\pi} \right] \end{split}$$

References

- [1] Ye L and Ye Z. Effects of shock location on aeroelastic stability of flexible panel. *AIAA Journal*, 56(9):3732–3744, 2018.
- [2] He Y, Shi A, Dowell E H, and Li X. Panel aeroelastic stability in irregular shock reflection. *AIAA Journal*, 60(11):6490–6499, 2022.
- [3] Ye L, Ye Z, and Wang X. Aeroelastic stability analysis of heated flexible panel subjected to an oblique shock. *Chinese Journal of Aeronautics*, 31(8):1650–1666, 2018.

Effects of shock impingement location on panel aeroelastic stability in Mach reflection

- [4] Dowell E H. Flutter of a buckled plate as an example of chaotic motion of a deterministic autonomous system. *Journal of Sound and Vibration*, 85(3):333–344, 1982.
- [5] Dowell E H. Observation and evolution of chaos for an autonomous system. *Journal of Applied Mechanics*, 51(3):664–673, 09 1984.
- [6] Pourtakdoust S H and Fazelzadeh S A. Chaotic analysis of nonlinear viscoelastic panel flutter in supersonic flow. *Nonlinear Dynamics*, 32:387–404, 2003.
- [7] Xie D, Xu M, and Dai H. Effects of damage parametric changes on the aeroelastic behaviors of a damaged panel. *Nonlinear Dynamics*, 97:1035–1050, 2019.
- [8] Li P and Yang Y. On the stability and chaos of a plate with motion constraints subjected to subsonic flow. *International Journal of Non-Linear Mechanics*, 59:28–36, 2014.
- [9] Brouwer K R, Perez R A, Beberniss T J, Spottswood S M, Ehrhardt D A, and Wiebe R. Investigation of aeroelastic instabilities for a thin panel in turbulent flow. *Nonlinear Dynamics*, 104:3323–3346, 2021.
- [10] Xue D Y and Mei C. Finite element nonlinear panel flutter with arbitrary temperatures in supersonic flow. *AIAA Journal*, 31(1):154–162, 1993.
- [11] Xue D Y and Mei C. Finite element nonlinear flutter and fatigue life of two-dimensional panels with temperature effects. *Journal of Aircraft*, 30(6):993–1000, 1993.
- [12] He Y, Shi A, and Dowell E H. Panel aeroelastic hysteresis induced by shock-reflection transition. *AIAA Journal*, 62(1):418–427, 2024.
- [13] Bolotin V V, Grishko A A, and Petrovsky A V. Secondary bifurcations and global instability of an aeroelastic non-linear system in the divergence domain. *Journal of Sound and Vibration*, 191(3):431–451, 1996.
- [14] Zhou J, Yang Z, and Gu Y. Aeroelastic stability analysis of heated panel with aerodynamic loading on both surfaces. *Science China Technological Sciences*, 55:2720–2726, 2012.
- [15] Dowell E H. Nonlinear oscillations of a fluttering plate. AIAA Journal, 4(7):1267–1275, 1966.
- [16] Ye L and Ye Z. Effects of shock location on aeroelastic stability of flexible panel. *AIAA Journal*, 56(9):3732–3744, 2018.
- [17] Shinde V, McNamara J, Gaitonde D, Barnes C, and Visbal M. Transitional shock wave boundary layer interaction over a flexible panel. *Journal of Fluids and Structures*, 90:263–285, 2019.
- [18] Shinde V, McNamara J, and Gaitonde D. Dynamic interaction between shock wave turbulent boundary layer and flexible panel. *Journal of Fluids and Structures*, 113:103660, 2022.
- [19] Taira K, Brunton S L, Dawson S T M, Rowley C W, Colonius T, McKeon B J, Schmidt O T, Gordeyev S, Theofilis V, and Ukeiley L S. Modal analysis of fluid flows: An overview. AIAA Journal, 55(12):4013–4041, 2017.